

# PERTURBED FACTOR ANALYSIS: IMPROVING GENERALIZABILITY ACROSS STUDIES

BY ARKAPRAVA ROY\*, ISAAC LAVINE\*, AMY H. HERRING\* AND DAVID  
B. DUNSON\*

*Duke University\**

Factor analysis is routinely used for dimensionality reduction. However, a major issue is ‘brittleness’ in which one can obtain substantially different factors in analyzing similar datasets. Factor models have been developed for multi-study data by using additive expansions incorporating common and study-specific factors. However, allowing study-specific factors runs counter to the goal of producing a single set of factors that hold across studies. As an alternative, we propose a class of Perturbed Factor Analysis (PFA) models that assume a common factor structure across studies after perturbing the data via multiplication by a study-specific matrix. Bayesian inference algorithms can be easily modified in this case by using a matrix normal hierarchical model for the perturbation matrices. The resulting model is just as flexible as current approaches in allowing arbitrarily large differences across studies, but has substantial advantages that we illustrate in simulation studies and an application to NHANES data. We additionally show advantages of PFA in single study data analyses in which we assign each individual their own perturbation matrix, including reduced generalization error and improved identifiability.

**1. Introduction.** Factor models are routinely used to characterize high dimensional, correlated data. The most commonly used factor model for  $p$ -variate data  $Y_i = (Y_{i1}, \dots, Y_{ip})^T$  is

$$(1.1) \quad Y_i = \Lambda \eta_i + \epsilon_i, \quad \eta_i \sim N_k(0, I), \quad \epsilon_i \sim N_p(0, \Sigma_1),$$

where it is assumed that data are centered prior to analysis,  $\eta_i = (\eta_{i1}, \dots, \eta_{ik})^T$  are latent factors,  $\Lambda$  is a  $p \times k$  factor loadings matrix, and  $\Sigma_1 = \text{diag}(\sigma_{11}^2, \dots, \sigma_{1p}^2)$  is a diagonal matrix of residual variances. Then the overall covariance matrix of the data is  $\Sigma = \Lambda \Lambda^T + \Sigma_1$ .

We are particularly motivated to analyze phthalate concentrations in blood or urine across demographic groups, collected in the National Health and Nutrition Examination Survey (NHANES). Exposures to phthalates

---

*Keywords and phrases:* Bayesian, Factor analysis, Generalizability, Hierarchical model, Meta analysis, Perturbation matrix, Robustness

are ubiquitous. They are present in soft plastics, including vinyl floors, toys and food packaging. Medical supplies such as blood bags and tubes contain phthalates. They are also found in fragrant products such as soap, shampoo, lotion, perfume and scented cosmetics. Because metabolites of a single parent compound or chemicals in the same family are often moderately to highly correlated, it is common to attempt to identify a small set of underlying factors (for example [Weissenburger-Moser et al. \(2017\)](#)). Epidemiologists are interested in interpreting these factors and in using them in analyses relating exposures to health outcomes. However, our collaborators have noticed a tendency to estimate very different factors in applying factor analysis to similar datasets or groups of individuals. For reliable interpretability and generalizability, it is important to reduce this brittleness and may be desirable to have a method that can produce a single set of factors that hold across groups.

There has been work on developing factor analysis methods that are robust in the presence of outliers ([Pison et al., 2003](#)). However, our motivation is different. Previous work extending factor analysis to multiple groups has focused on estimation of shared covariance structure. Simple methods include extensions of PCA to multiple groups, while more recently many customized methods have been developed. A key contribution was JIVE (Joint and Individual Variation Explained), which identifies low-rank covariance structure that is shared among multiple data types collected for the same subject ([Lock et al., 2013](#); [Feng, Hannig and Marron, 2015](#); [Feng et al., 2018](#)). In a Bayesian framework, [Roy, Schaich-Borg and Dunson \(2019\)](#) proposed TACIFA (Time Aligned Common and Individual Factor Analysis) for a related problem. Other methods include MSFA and BMSFA (Bayesian Multi-study Factor Analysis), which include inference over the number of shared latent factors. BMSFA takes a Bayesian approach to sampling  $\Lambda$ , focusing on situations with  $p \gg n$ , and uses a new post-hoc method for recovering the loadings matrix ([Aßmann, Boysen-Hogrefe and Pape, 2016](#); [De Vito et al., 2018](#)). In these approaches, the total covariance is decomposed into three parts, a common/shared covariance, a group-specific covariance and an error or residual variance. One drawback to these methods is the computational complexity of determining the number of shared versus group-specific factors.

We aim to identify a single set of factors under the assumption that the data in each group can be aligned to a common latent space via multiplication by a perturbation matrix. We represent the perturbed covariance in group  $j$  as  $Q_j \Sigma Q_j^T$ , where  $\Sigma$  is the common covariance, and  $Q_j$  is the group-specific perturbation matrix. As in the common factor model in [\(1.1\)](#), the

overall covariance  $\Sigma$  can be decomposed into a component due to common factors and a residual variance. The utility of the perturbation model also extends beyond multi-group settings. In the common factor model, the error terms only account for additive measurement error. We can obtain robust estimates of factor loadings in a single dataset by allowing for observation-specific perturbations. This accounts for both multiplicative and additive measurement error. In this case, we define separate  $Q_i$ 's for each data vector  $Y_i$ . Here  $Q_i$ 's are multiplicative random effects with mean  $I_p$ . Thus,  $E(Q_i Y_i) = E(Y_i)$  and the covariance structure on  $Q_i$  would determine the variability of  $Q_i Y_i$ .

Another challenge in factor analysis is non-identifiability. In particular, due to non-identifiability of the loading matrices and factors of (1.1), posterior samples of the loading matrices are not interpretable without identifiability restrictions (Seber, 2009; Lopes and West, 2004; Ročková and George, 2016; Fruehwirth-Schnatter and Lopes, 2018). Instead of imposing arbitrary constraints, with corresponding computational complications, a common technique is post-processing an unconstrained MCMC chain (Aßmann, Boysen-Hogrefe and Pape, 2016; Roy, Schaich-Borg and Dunson, 2019). Aßmann, Boysen-Hogrefe and Pape (2016) calculate a post-processing estimate by solving an Orthogonal Procrustes problem, but without uncertainty quantification (UQ). Roy, Schaich-Borg and Dunson (2019) propose post-processing the entire MCMC chain iteratively to be able to draw inference with UQ. The latent factors in our model are assumed to be heteroscedastic, unlike in the usual factor model in (1.1). This removes rotational ambiguity in the loading matrix, except for permutations, and helps to estimate loading matrices much more accurately even without any post-processing. We find this heteroscedastic model can also improve performance in estimating the covariance.

The next section describes the data and the model in detail. In Section 3, prior specifications are discussed. Our computational scheme is outlined in Section 4. We study the performance of our method in different simulation setups in Section 5. Section 6 considers an application to NHANES data. We end with some concluding remarks in Section 7.

**2. Data description and modeling.** In the National Health and Nutrition Examination Survey (NHANES), chemical levels in urine are recorded over the span 2009 to 2013 for 2749 individuals. We consider in total eight phthalate metabolite chemicals, Mono-n-butyl (MnBP), Mono-isobutyl (MiBP), Mono-ethyl (MEP), Mono-benzyl (MBeP), Mono-2-ethyl-5-carboxypentyl (MECPP), Mono-(2-ethyl-5-hydroxyhexyl) (MEHHP), Mono-(2-ethyl-5-oxohexyl)

(MEOHP) and Mono-(2-ethyl)-hexyl (MEHP), and 5 racial groups, Group 1: Mexican American (Mex), Group 2: Other Hispanic (OH), Group 3: Non-Hispanic White (N-H White), Group 4: Non-Hispanic Black (N-H Black) and Group 5: Other Race (Other/Multi) - Including Multi-Racial. We consider race and ethnicity because previous work has shown differences in patterns of use of products that contain phthalates (Taylor et al., 2018) and in measured phthalate concentrations (James-Todd et al., 2017) across racial or ethnic groups. Excess levels of phthalates in blood/urine have been linked to a variety of health outcomes, including obesity (Zhang et al., 2014; Kim and Park, 2014; Benjamin et al., 2017).

TABLE 1  
*Comparison across different groups in terms of number of participants and average chemical levels along with standard deviations in brackets.*

	Mex	OH	N-H White	N-H Black	Other/Multi
Number of participants	566	293	1206	516	168
MnBP	3.85 (1.96)	4.31 (4.96)	3.56 (2.17)	4.21 (1.81)	3.76 (2.11)
MiBP	2.88 (1.36)	3.21 (1.70)	2.52 (1.20)	3.47 (1.67)	2.79 (1.21)
MEP	8.32 (6.64)	9.51 (6.99)	6.91 (5.43)	11.16 (9.38)	7.33 (7.57)
MBeP	2.79 (1.58)	2.78 (1.61)	2.70 (1.67)	3.06 (1.77)	2.56 (1.68)
MECPP	4.80 (3.68)	4.55 (2.68)	4.16 (2.40)	4.36 (2.38)	4.34 (2.64)
MEHHP	3.83 (3.01)	3.73 (2.59)	3.45 (2.25)	3.79 (2.26)	3.57 (2.45)
MEOHP	3.11 (2.41)	3.00 (1.92)	2.79 (1.69)	3.05 (1.71)	2.86 (1.86)
MEHP	1.58 (1.23)	1.59 (1.29)	1.33 (0.89)	1.61 (0.99)	1.58 (1.31)

TABLE 2  
*Hotelling  $T^2$  statistic between phthalate levels for each pair of groups.*

	Mex	OH	N-H White	N-H Black	Other/Multi
Mex	0.00	31.84	108.59	191.93	28.04
OH	31.84	0.00	156.45	63.48	28.69
N-H White	108.59	156.45	0.00	409.64	55.51
N-H Black	191.93	63.48	409.64	0.00	101.90
Other/Multi	28.04	28.69	55.51	101.90	0.00

We provide a summary of the average chemical level across different groups in Table 1. In Table 2, we compute Hotelling  $T^2$  statistic between each pair of groups. The three groups Mex, OH and Other/Multi seem to

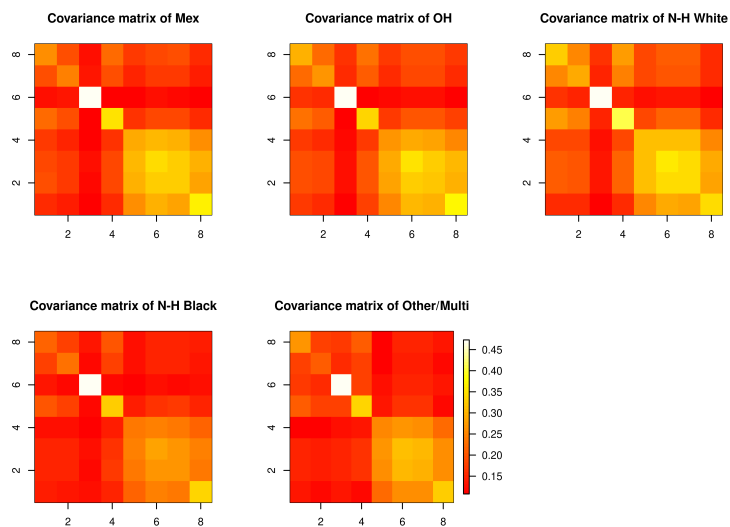


FIG 1. *Plots of the covariance matrices of the phthalate chemicals across different ethnic groups for NHANES data.*

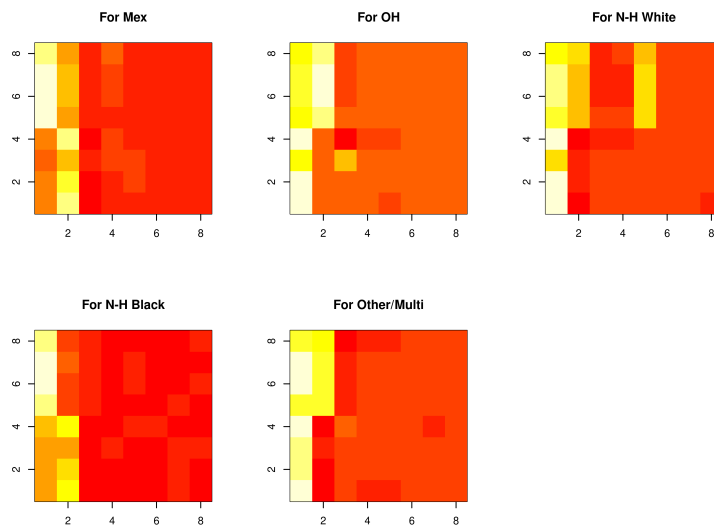


FIG 2. *Estimated loading matrices for different racial groups.*

be closer to each other than the other two groups. For each phthalate level, we also fit a one-way ANOVA model to determine differences across the groups taking the group Mex as baseline. The results are included in Tables 10 to 17 in Section 7. For almost all the cases, effect of the group N-H White is significantly different from the others. We plot group specific covariances in Figure 1. It is evident that there are shared structures with minor differences across the groups. However, the estimated loading matrices are different when we fit the common factor model in (1.1) separately for each group. In the next subsection, we propose a novel methodology for multi-group factor analysis to identify the common factors.

2.1. *Multi-group model.* Assume that we observe multiple groups, with the “groups” corresponding to different studies, batches of data, or levels of a covariate within a single study. Each  $p$ -dimensional response  $Y_{ij}$ , belonging to group  $G_j$ , for  $j \in 1 : J$  and  $i \in 1 : n_j$ , is modeled as:

$$(2.1) \quad \begin{aligned} Q_j Y_{ij} &= \Lambda \eta_{ij} + \epsilon_{ij}, \\ Q_j &\sim \text{MN}_{p \times p}(I_p, U, V), \quad \eta_{ij} \sim N(0, \Sigma_2), \\ \epsilon_{ij} &\sim N(0, \Sigma_1). \end{aligned}$$

The perturbation matrices  $Q_j$  are of dimension  $p \times p$ , and follow a matrix normal distribution, with diagonal row and column covariances  $U = V = \alpha I_p$ . The latent factors  $\eta_{ij}$  are heteroscedastic, so that  $\Sigma_2$  is diagonal with non-identical entries. We discuss the advantages of choosing heteroscedastic latent factors in more detail in Section 2.3. After integrating out the latent factors, the observations are marginally distributed as  $Y_{ij} \sim \text{MVN}(0, Q_j^{-1}[\Lambda \Sigma_2 \Lambda^T + \Sigma_1](Q_j^{-1})^T)$ . If we write  $Q_j^{-1} = I_p + \Psi_j$ , then  $\Lambda$  is the shared loadings matrix, and  $\Psi_j \Lambda$  is a group-specific loadings matrix. We can quantify the magnitude of perturbation as  $\|\Psi_j\|_F$ , where  $\|\cdot\|_F$  stands for the Frobenius norm. For identifiability of  $Q_j$ 's, we consider  $Q_1 = I_p$  and  $n_1 \geq 2$ . We call our model Perturbed Factor Analysis (PFA).

2.1.1. *Model properties.* Let  $\Omega_1$  and  $\Omega_2$  be two positive definite (p.d.) matrices. Then there exist non-singular matrices  $A$  and  $B$ , where  $\Omega_1 = AA^T$  and  $\Omega_2 = BB^T$ . By choosing  $E = AB^{-1}$ , we have  $\Omega_1 = E\Omega_2E^T$ . If the two matrices  $\Omega_1$  and  $\Omega_2$  are close, then  $E$  will be close to the identity. However,  $E$  is not required to be symmetric. In our multi-group model in (2.1), the  $Q_j$ s allow for small perturbations around the shared covariance matrix  $\Sigma = \Lambda \Sigma_2 \Lambda^T + \Sigma_1$ . We define the following class for the  $Q_j$ 's,

$$\mathcal{C}_\epsilon = \{Q : \|Q - I_p\|_F \leq \epsilon\}.$$

The index  $\epsilon$  controls the amount of deviation across groups. In (2.1) we define  $U = V = \alpha I_p = V$ , for some small  $\alpha$ , which we call the perturbation parameter. By choosing  $U = V$  to be diagonal with identical entries, we impose uniform perturbation across all the rows and columns around  $I_p$ . However, the perturbation matrices themselves are not required to be symmetric.

LEMMA 1.  $P(Q_i \notin \mathcal{C}_\epsilon) \leq \exp(-\epsilon^2/2\alpha^2)$ .

The proof follows from Chebychev’s inequality. This result allows us to summarize the level of induced perturbation for any given  $\alpha$ . Using this lemma, we can show the following corollary.

LEMMA 2.

$$\begin{aligned} & KL(N(0, Q_j^{-1}[\Lambda\Sigma_2\Lambda^T + \Sigma_1](Q_j^{-1})^T), N(0, Q_l^{-1}[\Lambda\Sigma_2\Lambda^T + \Sigma_1](Q_l^{-1})^T)) \\ & \lesssim \left| \|Q_j^{-1}\|_F^2 - \|Q_l^{-1}\|_F^2 \right|. \end{aligned}$$

Therefore the Kullback-Leibler divergence between the marginal distributions of any two groups  $j$  and  $l$  can be bounded by  $\left| \|Q_j^{-1}\|_F^2 - \|Q_l^{-1}\|_F^2 \right|$  up to some constant. We define a divergence statistic between groups  $j$  and  $l$  as  $d_{jl} = \sqrt{\frac{\left| \|Q_j^{-1}\|_F^2 - \|Q_l^{-1}\|_F^2 \right|}{p^2}}$ . This generates a divergence matrix  $D = (\{d_{jl}\})$ , where larger  $d_{jl}$  imply a greater difference between the two groups.

In our multi-group model, there is no computational complication regarding specification of the ranks of the shared and individual spaces unlike other methods. We can directly rely on current methods for accommodating unknown number of factors in the single group setting (Bhattacharya and Dunson, 2011). Also, computationally our method is faster than other multi-group factor models such as BMSFA due to smaller number of parameters, and better identifiability, leading to better mixing of Markov Chain Monte Carlo (MCMC).

2.1.2. *Tuning the parameter  $\alpha$  for multi-group data.* The hyper-parameter  $\alpha$  controls the level of perturbation across groups. In Section 5, we show that properly tuning  $\alpha$  is necessary to obtain accurate estimates of the loading matrix  $\Lambda$ . We propose a cross validation technique to choose the optimal  $\alpha$ . We randomly divide each group 50/50 into training and test sets. Then for a range of  $\alpha$  values, we fit the model on the training data, and calculate the predictive log-likelihood of the test set. After integrating out the latent factors, the predictive distribution is  $Q_j Y_{ij} \sim N(0, \Lambda\Sigma_2\Lambda^T + \Sigma_1)$ . If there are

multiple values of  $\alpha$  with similar predictive log-likelihoods, then the smallest  $\alpha$  is chosen as optimal.

Alternatively, we can take a fully Bayesian approach and put a prior on  $\alpha$ . We call this method Fully Bayesian Perturbed Factor Analysis (FBPFA). We see that FBPFA performs similarly to PFA in practice. FBPFA involves a slightly more complex MCMC implementation. PFA avoids sensitivity to the prior for  $\alpha$  but requires the computational overhead of cross validation, and can potentially be less efficient in requiring a hold out sample, while also not characterizing uncertainty in estimating  $\alpha$ .

**2.1.3. Posterior consistency.** Let  $\Theta_\Lambda, \Theta_{\Sigma_1}, \Theta_{\Sigma_2}$  be the parameter spaces of  $\Lambda, \Sigma_1$  and  $\Sigma_2$ , respectively,  $\Theta$  be the set of  $p \times p$  positive semidefinite matrices corresponding to the parameter space of  $\Sigma$ , and  $\mathcal{Q}_j$  be the parameter space of  $Q_j$ . Let  $\Pi_\Lambda, \Pi_{\Sigma_1}, \Pi_{\Sigma_2}, \Pi_Q$  be the priors for  $\Lambda, \Sigma_1, \Sigma_2$  and  $Q_j$ 's. We restate some of the results from [Bhattacharya and Dunson \(2011\)](#) for our modified factor model. With minor modification, the proofs will remain the same.

Let  $g : \Theta_\Lambda \times \Theta_{\Sigma_1} \times \Theta_{\Sigma_2} \rightarrow \Theta_\Sigma$  be a continuous map such that  $g(\Lambda, \Sigma_1, \Sigma_2) = \Lambda^T \Sigma_2 \Lambda + \Sigma_1$ .

**LEMMA 3.** *For any  $(\Lambda, \Sigma_1, \Sigma_2) \in \Theta_\Lambda \times \Theta_{\Sigma_1} \times \Theta_{\Sigma_2}$ , we have  $g(\Lambda, \Sigma_1, \Sigma_2) \in \Theta_\Sigma$ .*

The proof is similar to Lemma 1 of [Bhattacharya and Dunson \(2011\)](#). In our Bayesian approach, we choose independent priors for  $\Lambda, \Sigma_1$  and  $\Sigma_2$  and that induces a prior on  $\Sigma$  through the map  $g$ . We also have following proposition.

**PROPOSITION 4.** *If  $(\Lambda, \Sigma_1, \Sigma_2) \sim \Pi_\Lambda \otimes \Pi_{\Sigma_1} \otimes \Pi_{\Sigma_2}$ , then  $\Pi_\Lambda \otimes \Pi_{\Sigma_1} \otimes \Pi_{\Sigma_2}(\Theta_\Lambda \times \Theta_{\Sigma_1} \times \Theta_{\Sigma_2}) = 1$ .*

The proof is similar to Proposition 1 of [Bhattacharya and Dunson \(2011\)](#) with minor modifications. Now, we proceed to establish that the posterior of our multigroup model is weakly consistent under a fixed  $p$  and increasing  $n$  regime. Let us assume that the complete parameter space is  $\kappa = (\Lambda, \Sigma_1, \Sigma_2, Q_2, \dots, Q_j)$  and let  $\kappa_0$  be the truth for  $\kappa$ .

*Assumptions:*

1. For some  $M > 0$ , the true perturbation matrices are  $Q_{j0} \in \mathcal{C}_M$ , with  $\mathcal{C}_M$  defined in Section [2.1.1](#).



2. There exists some  $E > 0$ ,  $F_1 > 0$  and  $F_2 > 0$  such that  $\max_{ij} |\Lambda_0| < E$  and  $F_1 < \Sigma_{20k} < F_2$  for all  $k = 1, \dots, r$ .

**THEOREM 5.** *Under Assumptions 1-2, the posterior for  $\kappa$  is weakly consistent at  $\kappa_0$ .*

We first show that our proposed prior has large support in the sense that the truth belongs to the Kullback-Leibler support of the prior. Thus the posterior probability of any neighbourhood around the truth converges to one in  $P_{\kappa_0}^{(n)}$ -probability as  $n$  goes to  $\infty$  as a consequence of [Schwartz \(1965\)](#). Here  $P_{\kappa}^{(n)}$  is the distribution of a sample of  $n$  observations with parameter  $\kappa$ . Hence, the posterior is weakly consistent. The proof is in [Section 7](#).

**2.2. Measurement-error model.** We can modify the multi-group model to obtain improved factor estimates on a single dataset by considering observation-level perturbations. Here we observe  $Y_{ij}$ 's for  $j = 1, \dots, m_i$ , which are  $m_i$  many proxies of true observation  $W_i$  with multiplicative measurement errors  $Q_{ij}^{-1}$ 's such that  $W_i = Q_{ij}Y_{ij}$ . The modified factor model is

$$(2.2) \quad \begin{aligned} Q_{ij}Y_{ij} &= \Lambda\eta_{ij} + \epsilon_{ij}, \quad \epsilon_{ij} \sim N(0, \Sigma_1), \\ Q_{ij} &\sim \text{MN}_{p \times p}(I_p, U, V) \quad \eta_i \sim N(0, \Sigma_2). \end{aligned}$$

In this model, the  $Q_{ij}$ 's apply a multiplicative perturbation to each data vector. We have  $Y_{ij} = Q_{ij}^{-1}W_i$  where  $Q_{ij}^{-1}$  is a matrix. Thus, here the measurement errors are  $U_{ij} = (Q_{ij}^{-1} - I_p)W_i$  and  $E(U_{ij}|W_i) = 0$ . This model is different from the multiplicative measurement error model of [Sarkar et al. \(2018\)](#). In [Sarkar et al. \(2018\)](#), observations  $Y_{ij}$ 's are modeled as  $Y_{ij} = W_i \circ U_{ij}$ , where  $\circ$  denotes the element wise dot product and  $U_{ij}$ 's are independent of  $W_i$  with  $E(U_{ij}) = 1$ . Thus, the measurement error in the  $l$ -th component (i.e.  $U_{ijl}$ ) is dependent on  $W_i$  primarily through  $W_{il}$ . However in our construction, it depends on the entire vector  $W_i$ . Thus, the measurement errors are a linear function of the entire true observation  $W_i$ .

This is a much more general setup than [Sarkar et al. \(2018\)](#). The identifiability of distributions of  $Q_{ij}$  and  $Y_{ij}$  is difficult. For simplicity, we again assume  $U = V = \alpha I_p$ . In this case we have,

$$\begin{aligned} E(Q_{ij}Y_{ij}) &= 0 \\ V(Q_{ij}Y_{ij}) &= E(V(Q_{ij}Y_{ij}|Q_{ij})) + V(E(Q_{ij}Y_{ij}|Q_{ij})) \\ &= E(V(Q_{ij}Y_{ij}|Q_{ij})) + 0 = \alpha^2 dI_p + \Sigma, \quad d = \sum_{k=1}^p \Sigma_{kk} \end{aligned}$$

Thus, only the diagonal elements of  $\Sigma$  are not identifiable and the perturbation parameter  $\alpha$  does not influence the dependence structure among the variables. Hence, with our heteroscedastic latent factors we can still recover the loading structure. To tune  $\alpha$ , we can use the marginal distributions  $Q_{ij}Y_{ij} \sim \text{MVN}(0, \alpha^2 dI_p + \Sigma)$  to develop a cross validation technique when  $m_i > 1$  for all  $i = 1, \dots, n$  as in Section 2.1.2. However, when  $m_i = 1$  for all  $i$ , this is not possible. Thus, we propose to estimate  $\alpha$  as in FBPFA by using a weakly informative prior concentrated on small values, while assessing sensitivity to hyperparameter choice.

2.3. *The special case  $Q_j = I_p$  for all  $j$ .* For a single study dataset without any measurement error, we can modify our PFA method by taking  $Q_j = I_p$  for all  $j$ . Then the model reduces to a traditional factor model with heteroscedastic latent factors:

$$(2.3) \quad \begin{aligned} Y_i &= \Lambda \eta_i + \epsilon_i, & \epsilon_i &\sim N(0, \Sigma_1) \\ \eta_i &\sim N(0, \Sigma_2), \end{aligned}$$

where  $\Sigma_2$  is assumed to be diagonal with non-identical entries. Integrating out the latent factors, the marginal likelihood is  $Y_i \sim \text{MVN}(0, \Lambda \Sigma_2 \Lambda^T + \Sigma_1)$ . Except for the diagonal matrix  $\Sigma_2$ , the marginal likelihood is almost similar to the marginal likelihood for a traditional factor model. As  $\Sigma_2$  has non-identical diagonal entries, the likelihood is no longer invariant under arbitrary rotations. For the factor model in 1.1,  $(\Lambda, \eta)$  and  $(\Lambda R, R^T \eta)$  have equivalent likelihood for any orthonormal matrix  $R$ . This is not the case in our model unless  $R$  is a permutation matrix. Thus, this simple modification over the traditional factor model helps to efficiently recover the true loading structure. This is demonstrated in Case 1 of Section 5. We can also show that the posterior is weakly consistent based on the results established in Section 2.1.3.

**3. Prior.** As in [Bhattacharya and Dunson \(2011\)](#), we put the following prior on  $\Lambda$  to allow for automatic selection of rank and easy posterior computation:

$$\begin{aligned} \lambda_{lk} | \phi_{lk}, \tau_k &\sim N(0, \phi_{lk}^{-1} \tau_k^{-1}), \\ \phi_{lk} &\sim \text{Gamma}(\nu_1, \nu_1), \quad \tau_k = \prod_{i=1}^k \delta_i \\ \delta_{1,1} &\sim \text{Gamma}(\kappa_1, 1), \quad \delta_{1,i} \sim \text{Gamma}(\kappa_2, 1). \end{aligned}$$

The parameters  $\phi_{lk}$  control local shrinkage of the elements in  $\Lambda$ , whereas  $\tau_k$  controls global shrinkage of the  $k$ -th column. For  $\kappa_2 > 1$ , we have  $\tau_k$  stochastically increasing with  $k$ , which imposes greater shrinkage for columns with higher column index.

For the heteroscedastic latent factors, each diagonal element of  $\Sigma_2$  has an independent prior:

$$\sigma_{2i} \sim \text{IG}(d, 0.1)$$

for some constant  $d$ . In our simulations, we see that  $d$  does not influence much the predictive performance of our method. However, as  $d$  increases, it puts more shrinkage on the latent factors. We choose  $d = 10$  for most of our simulations. For the residual error variance  $\Sigma_1$ , we place a weakly information prior on the diagonal elements:

$$\sigma_{1i} \sim \text{IG}(0.1, 0.1).$$

In our simulations, weakly informative  $\text{IG}(0.1, 0.1)$  prior on  $\alpha$  works well to get good predictive performance and to estimate the loading structure, even for a single study dataset.

**4. Computation.** Posterior inference is straightforward with a Gibbs sampler, because all of the parameters have conjugate full conditional distributions. For the model in (2.1), the full conditional of the perturbation matrix  $Q_j$  is:

$$\text{vec}(Q_j)|Y \sim \text{MVN}(\Gamma_j(V \otimes U)^{-1}\text{vec}(I_p), \Gamma_j),$$

where  $\Gamma_j = [(V \otimes U)^{-1} + S_j \otimes \Sigma^{-1}]^{-1}$ , and  $S_j = \sum_i Y_{ij}Y_{ij}^T$ . The full conditionals for all other parameters are described in [Bhattacharya and Dunson \(2011\)](#), replacing  $Y_{ij}$  by  $Q_j Y_{ij}$ . For the model in (2.2), the full conditional of  $Q_{ij}$  is:

$$\text{vec}(Q_{ij})|Y \sim \text{MVN}(\Gamma_{ij}(V \otimes U)^{-1}\text{vec}(I_p), \Gamma_{ij}),$$

where  $\Gamma_{ij} = [(V \otimes U)^{-1} + S_{ij} \otimes \Sigma^{-1}]^{-1}$ , and  $S_j = Y_{ij}Y_{ij}^T$ . Other parameters can again be updated using the results in [Bhattacharya and Dunson \(2011\)](#) replacing  $Y_{ij}$  by  $Q_{ij}Y_{ij}$ . If we put a prior on  $\alpha$ , the posterior distribution of  $\alpha$  is given by  $\text{IG}(0.1 + (J-1)p^2, 0.1 + \sum_j \|Q_j - I_p\|_F^2)$  for the model in (2.1) and for the model in (2.2), the posterior distribution of  $\alpha$  is  $\text{IG}(0.1 + p^2 \sum_i m_i, 0.1 + \sum_{ij} \|Q_{ij} - I_p\|_F^2)$ .

**5. Simulation Study.** In this section, we study the performance of our method in various simulation settings. As ground truth, we consider the two loading matrices given in Figure 3. These are similar to the ones considered in Ročková and George (2016). The two loading matrices have equal number of columns which is 5. The first loading matrix has 21 rows and the second one has 128 rows. We compare the estimated loading matrices for different choices of hyperparameters. We investigate the perturbation parameter  $\alpha$  and the shape parameter  $d$ , which controls the level of shrinkage on the diagonal entries of  $\Sigma_2$ .

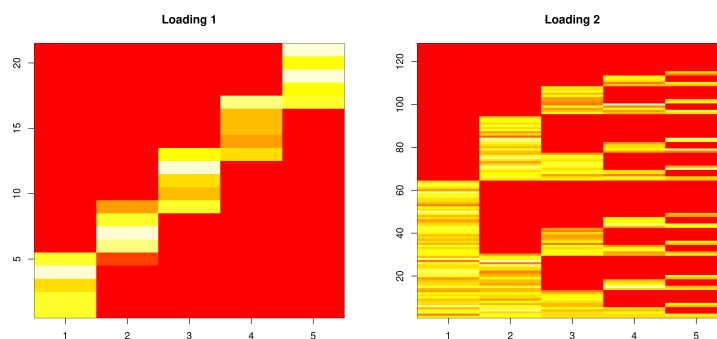


FIG 3. The ground truth loading matrices of dimension  $21 \times 5$  (Loading 1) and  $128 \times 5$  (Loading 2) respectively.

For the single dataset case, we compare with the approach of Bhattacharya and Dunson (2011) (B&D), which corresponds to the special case of our approach that fixes the perturbation matrices and latent factor covariances equal to the identity. A point estimate of the loading matrix for B&D is calculated by post-processing the posterior samples. We use the algorithm of Afmann, Boysen-Hogrefe and Pape (2016) to rotationally align the samples of  $\Lambda$ , as used in De Vito et al. (2018). In contrast, our method does not require any post-processing. We simply take the mean of the posterior samples to estimate the loading matrix. For the multi-group case, we compare our estimates with Bayesian Multi-study Factor Analysis (BMSFA), which also requires post-processing to remove rotational ambiguity. We use the MSFA package from <https://github.com/rdevito/MSFA>.

We compare the different methods using predictive likelihood. Simulated data are randomly divided 50/50 into training and test sets. After fitting each model on the training data, we calculate the predictive likelihood of the test set. All methods are run for 7000 iterations of the Gibbs sampler,

with 2000 burn-in samples. Each simulation is replicated 30 times.

5.1. *Case 1: Single dataset,  $Q_j = I_p$ .* We first consider factor analysis of a single dataset. Starting with the two loading matrices in Figure 3, we simulate latent factors from  $N(0, I_5)$ , and generate datasets of 500 observations, with residual variance  $\Sigma_1 = I_p$ . We compare B&D with our method when  $Q_j = I_p$ , so the only adjustment is to use heteroscedastic latent factors. Note that the simulated latent factors actually have identical variances.

In Table 3 and 4, we compare methods by MSE of the estimated versus true covariance matrix. For loading matrix 1, Bayesian FA had an MSE of 2.59, which is dominated by our method across a range of values of  $d$ .

TABLE 3  
MSE of estimated covariance matrix for loading matrix 1, across different values of  $d$

d	MSE
0.1	1.04
10	1.32
100	1.38

For loading matrix 2, Bayesian FA had a MSE of 10.81. Again, our method beats this across a range of values of  $d$ .

TABLE 4  
MSE of estimated covariance matrix for loading matrix 2, across different values of  $d$

d	MSE
0.1	5.21
10	9.45
100	10.32

We compare the estimated and true loading matrices in Figure 4. Our method performs overwhelmingly better at estimating the true loading structure compared with B&D FA. The first five columns of the estimated loadings based on our method are very close to the true loading structure under some permutation. Having heteroscedastic latent factors give us such improved performance.

5.2. *Case 2: Multi-group, multiplicative perturbation.* In this case, we simulate data from the multi-group model in (2.1) with  $m_i = 1$  for all  $i = 1, \dots, 500$ . First, observations  $Y_i$  are generated using the same method as in Case 1. The data are then split into 10 groups of 50 observations, such that  $G_j = \{Y_k : 50(j-1) \leq k \leq 50j\}$ . The groups are perturbed using matrices  $Q_{j0} \sim \text{MN}(I_p, \alpha_0 I_p, \alpha_0 I_p)$  for different choices of  $\alpha_0$ , setting  $Q_1 = I_p$ .

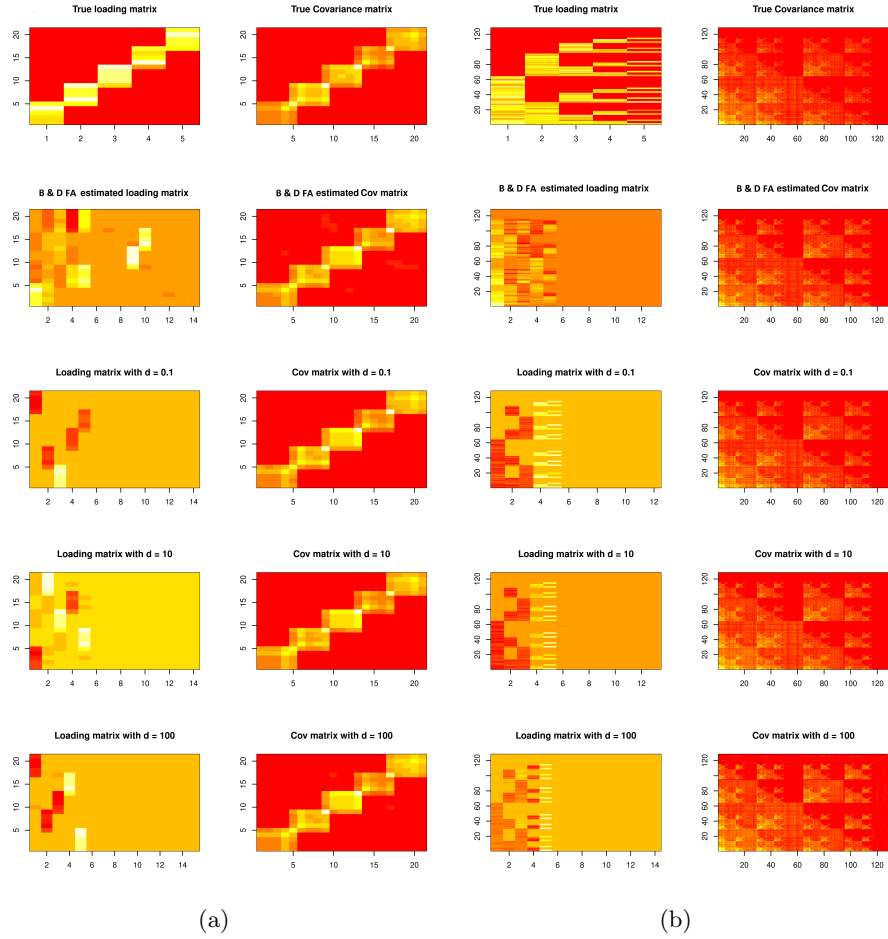


FIG 4. Comparison of true and estimated loading matrices and covariance matrices for Case 1. Comparison of B&D FA with our method for different choices of  $d$ . Results for loading matrix 1 are in (a) and 2 in (b). For all the cases, we fix  $Q_j = I$ .

TABLE 5  
Average predictive log-likelihood for PFA with optimal  $\alpha$ , FBPFA and BMSFA in Simulation Case 2.

True Loading	$\alpha_0$	PFA for optimal $\alpha$	FBPFA	BMSFA
Loading 1	$1 \times 10^{-4}$	-31.65	-25.92	-679.36
	$1 \times 10^{-2}$	-30.32	-26.01	-921.76
Loading 2	$1 \times 10^{-4}$	-210.43	-251.13	-6871.38
	$1 \times 10^{-2}$	-351.42	-304.10	-25018.50

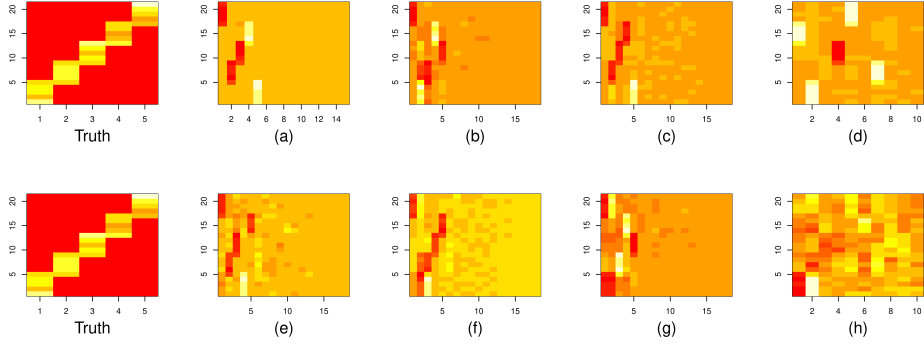


FIG 5. Comparison of estimated loading matrix 1 in Simulation Case 2 with different choices of  $\alpha_0$  and  $\alpha$  where  $Q_{j0} \sim MN(I_p, \alpha_0 I_p, \alpha_0 I_p)$  and  $U = \alpha I_p = V$ . (a) Estimated loading for  $\alpha = 1 \times 10^{-4}, \alpha_0 = 1 \times 10^{-4}$ , (b) For  $\alpha = 1 \times 10^{-2}, \alpha_0 = 1 \times 10^{-4}$ , (c) For FBPFA with  $\alpha_0 = 1 \times 10^{-4}$ , (d) For BMSFA with  $\alpha_0 = 1 \times 10^{-4}$ , (e) For  $\alpha = 1 \times 10^{-4}, \alpha_0 = 1 \times 10^{-2}$ , (f) For  $\alpha = 1 \times 10^{-2}, \alpha_0 = 1 \times 10^{-2}$ , For FBPFA with  $\alpha_0 = 1 \times 10^{-2}$ , (h) For BMSFA with  $\alpha_0 = 1 \times 10^{-2}$ .

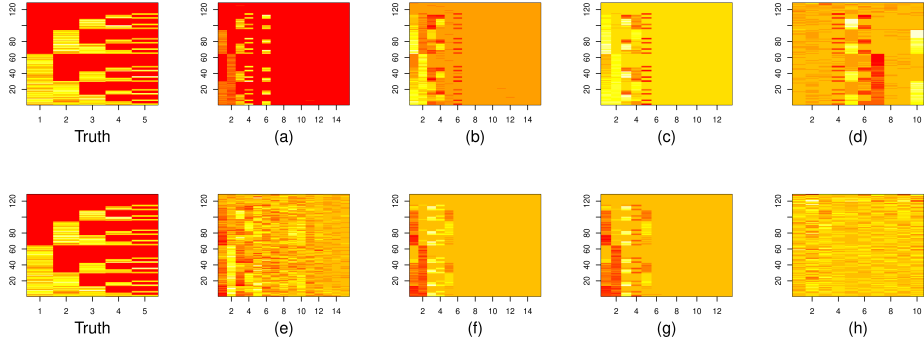


FIG 6. Comparison of estimated loading for loading matrix 2 in Simulation Case 2 with different choices of  $\alpha_0$  and  $\alpha$  where  $Q_{j0} \sim MN(I_p, \alpha_0 I_p, \alpha_0 I_p)$  and  $U = \alpha I_p = V$ . (a) Estimated loading for  $\alpha = 1 \times 10^{-4}, \alpha_0 = 1 \times 10^{-4}$ , (b) For  $\alpha = 1 \times 10^{-2}, \alpha_0 = 1 \times 10^{-4}$ , (c) For FBPFA with  $\alpha_0 = 1 \times 10^{-4}$ , (d) For BMSFA with  $\alpha_0 = 1 \times 10^{-4}$ , (e) For  $\alpha = 1 \times 10^{-4}, \alpha_0 = 1 \times 10^{-2}$ , (f) For  $\alpha = 1 \times 10^{-2}, \alpha_0 = 1 \times 10^{-2}$ , For FBPFA with  $\alpha_0 = 1 \times 10^{-2}$ , (h) For BMSFA with  $\alpha_0 = 1 \times 10^{-2}$ .

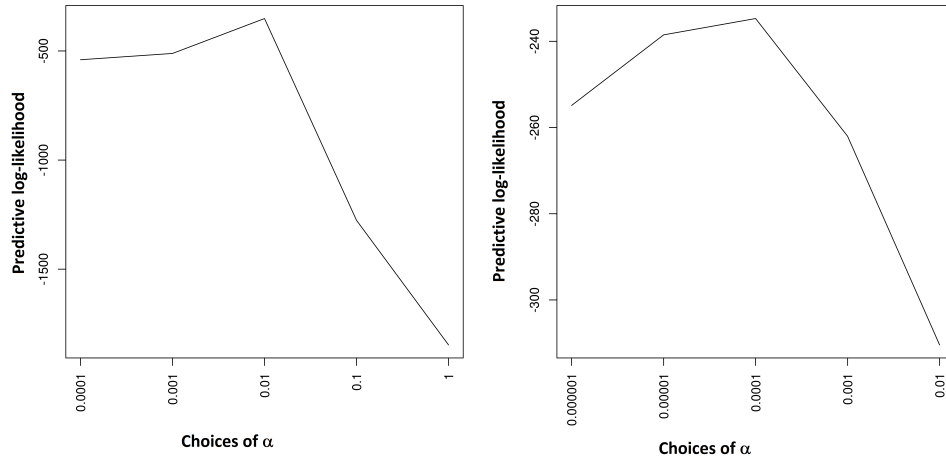


FIG 7. Average predictive log-likelihoods for different choices of  $\alpha$  in Simulation Case 2 for two cases where in the first case the perturbation matrices are generated using true  $\alpha_0 = 1 \times 10^{-2}$  and in the second case it is  $\alpha_0 = 1 \times 10^{-4}$ . This is based on the simulation experiment of Figure 6

Figures 5 and 6 show the estimated loading matrices. We can see that we obtain accurate estimates even when allowing for a higher level of perturbation than the truth,  $\alpha_0 \leq \alpha$ . However, the estimates are best when  $\alpha = \alpha_0 = 1 \times 10^{-4}$ . Performance degrades more sharply when we underestimate the level of perturbation, as in the case where  $\alpha = 1 \times 10^{-4}$ ,  $\alpha_0 = 1 \times 10^{-2}$ . The estimated loadings from PFA and FBPFSA are better than BMSFA. The number of factors is correctly identified by all the methods except for the case with higher perturbation using BMSFA. For all other cases, the estimated loadings matrix is close to the true loadings matrix under some permutation of the columns. In our method, considering only the first five columns of the estimated loadings is sufficient to accurately estimate the loading structure. All the other columns can be removed due to their very small contribution.

In Figure 7, we show the predictive likelihood under a range of  $\alpha$  values. This demonstrates the utility of our cross-validation technique to find the optimal  $\alpha$ . In Table 5, we compare the performance of PFA with optimal  $\alpha$ , FBPFSA and BMSFA in terms of predictive likelihood. PFA and FBPFSA have overwhelmingly better performance.

5.3. *Case 3: Multi-group, additive perturbation.* In Case 2, each group is multiplied by a unique perturbation matrix  $Q_j$ . In this case, we perturb



the data by adding a group specific loading matrix  $\Psi_j$  to a shared loading matrix  $\Lambda$ , as the model in (5.1).

$$(5.1) \quad \begin{aligned} Y_i &= (\Lambda + \Psi_j)\eta_i + \epsilon_{1i} \text{ and } Y_i \in G_j, \\ \epsilon_{1i} &\sim N(0, \Sigma_1) \quad \eta_i \sim N(0, I_p), \end{aligned}$$

where the group specific loadings ( $\Psi_j$ 's) are lower in magnitude in comparison to the shared loading matrix  $\Lambda$ . This can also be an alternative perturbation model. We consider two situations, the first generating elements of  $\Psi_j$  from  $N(-0.2, 0.2)$ , and the second from  $N(-0.5, 0.8)$ . The matrices  $\Psi_j$  are the same dimension as  $\Lambda$ . Figure 8 shows the true and estimated loading matrices from BMFSA, FBPFA and PFA across a range of values of  $\alpha$ . The estimated loadings from PFA are much closer to the truth than BMFSA. The number of factors is again correctly identified by all the methods except for the case with higher perturbation using BMSFA. Table 6 compares predictive likelihoods of the two methods in different cases, and again, PFA and FBPFA outperform BMSFA.

TABLE 6  
Average predictive log-likelihood for PFA for different choices of  $\alpha$ , FBPFA and BMSFA in Simulation Case 3.

Generative Distribution of $\Psi_j$ 's	True Loading	PFA for $\alpha = 1 \times 10^{-2}$	PFA for $\alpha = 1 \times 10^{-4}$	FBPFA	BMSFA
N(-0.2, 0.2)	Loading 1	-56.27	-60.71	-56.63	-429.28
	Loading 2	-1041.28	-361.82	-421.28	-5853.65
N(-0.5, 0.8)	Loading 1	-30.68	-50.09	-54.62	-514.67
	Loading 2	-320.04	-246.06	-479.59	-6798.37

5.4. *Case 4: Observation-level perturbations.* In this case, we generate data from the model in 2.2. First, a non-perturbed dataset is generated exactly the same way as in Case 1 and 2. Then, we generate separate perturbation matrices  $Q_{i0} \sim MN(I_p, \alpha_0 I_p, \alpha_0 I_p)$  for each data vector  $Y_i$ . We repeat this simulation for different choices of  $\alpha_0$ .

Figures 9 and 10 show the estimated loading when they are estimated using  $\alpha = 1 \times 10^{-4}$ . The method performs poorly when perturbation parameter  $\alpha$  is lower than true parameter  $\alpha_0$  as in the previous cases. Figure 11 illustrates performance of FBPFA in this case. When perturbation is higher, the performance deteriorates as it is more difficult to capture the loading structure accurately. However, number of factors is always identified correctly. Overall, our method is able to accurately estimate the true loading structure.

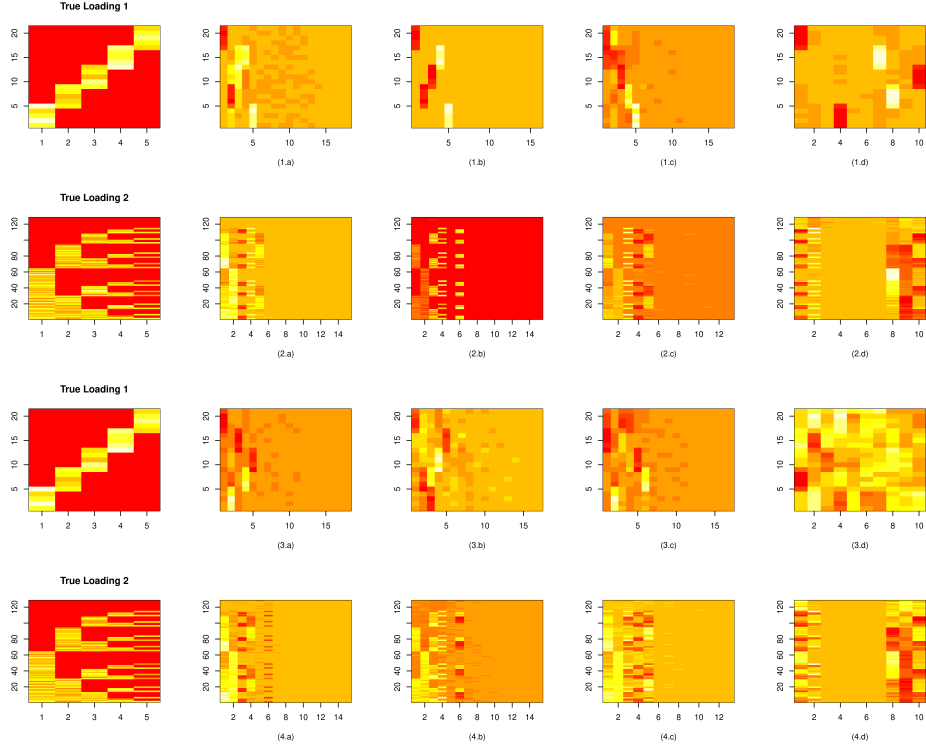
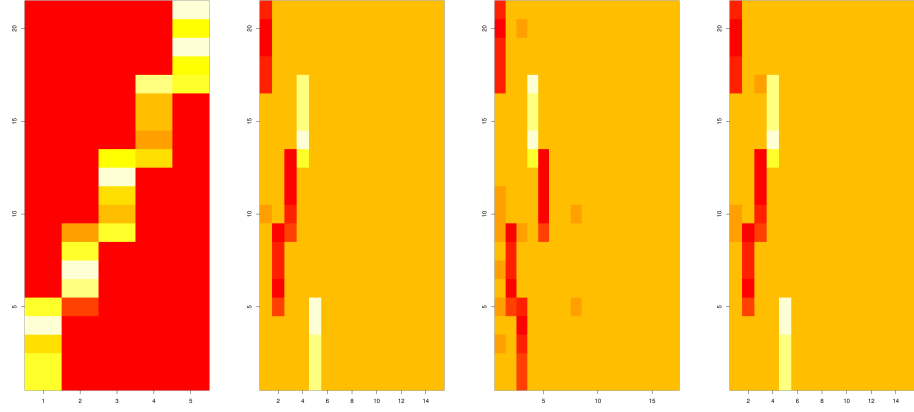
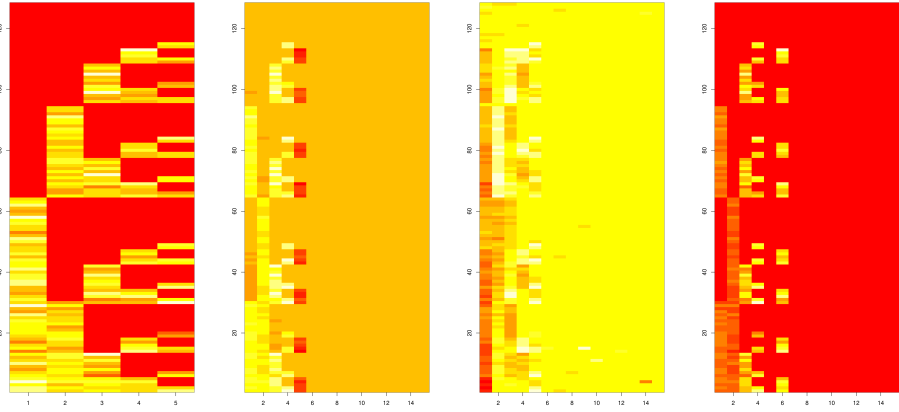


FIG 8. Comparison of estimated loading matrices in Simulation Case 3 with different choices of  $\alpha$  for both of the two choices of loading when group specific perturbations are added to the shared loading matrix by addition. The first two rows true  $\Psi_j$ 's are generated from  $N(-0.2, 0.2)$  and for the last two rows  $\Psi_j$ 's are generated from  $N(-0.5, 0.8)$  (a) Estimated loading for  $\alpha = 1 \times 10^{-2}$ , (b) Estimated loading for  $\alpha = 1 \times 10^{-4}$ , (c) Estimated loading for FBPFA.



(a) The true loading matrix (b) Estimated loading matrix when  $d = 100$  and  $\alpha_0 = 0.0001$  (c) Loading matrix when  $d = 100$  and  $\alpha_0 = 0.01$  (d) Loading matrix when  $d = 100$  and  $\alpha_0 = 0.00001$

FIG 9. Comparison of the estimated loading matrices in Simulation Case 4 for different prior choices of  $d$  and different true perturbation matrices  $Q_{i0}$ , where  $Q_{i0} \sim MN(I_p, \alpha_0 I_p, \alpha_0 I_p)$  and  $\alpha_0 = 1 \times 10^{-4}$ .



(a) The true loading matrix (b) Estimated loading matrix when  $d = 100$  and  $\alpha_0 = 0.0001$  (c) Loading matrix when  $d = 100$  and  $\alpha_0 = 0.01$  (d) Loading matrix when  $d = 100$  and  $\alpha_0 = 0.00001$

FIG 10. Comparison of the estimated loading matrices in Simulation Case 4 for different prior choices of  $d$  and different true perturbation matrices  $Q_{i0}$ , where  $Q_{i0} \sim MN(I_p, \alpha_0 I_p, \alpha_0 I_p)$  and  $\alpha_0 = 1 \times 10^{-4}$ .

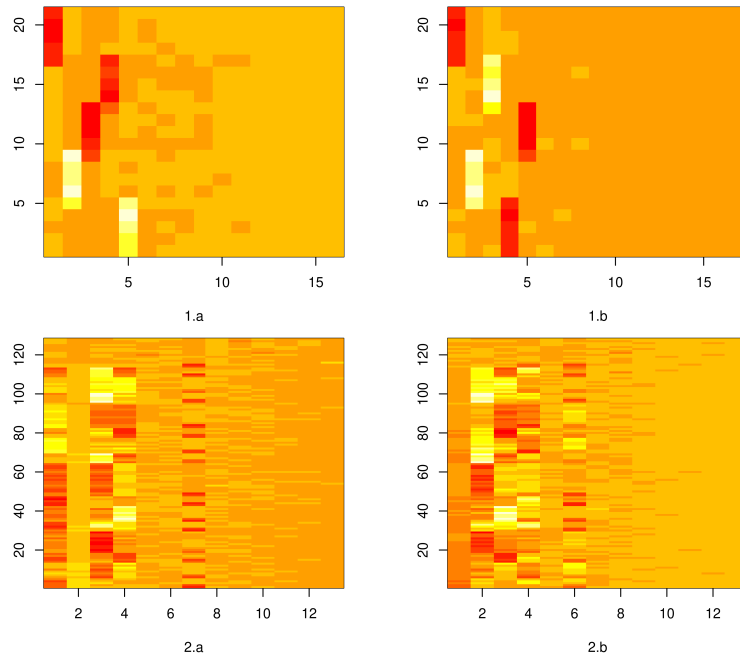


FIG 11. Estimated loadings using FBPFA for different choices of  $\alpha_0$  in Simulation Case 4 for two cases. (a): Estimated loading for  $\alpha_0 = 1 \times 10^{-4}$ , (b): For  $\alpha_0 = 1 \times 10^{-2}$ .

**6. Application to NHANES data.** We fit our model in (2.1) to the NHANES dataset as described in Section 2 to get a shared set of factors. In our analysis, we consider the standardized data and explore those shared structures. In this standardized data, the chemical levels are standardized across all the groups. For our analysis, the data are randomly split, with 2/3 as a training set, and 1/3 as a test set. We collect 5000 post burn MCMC samples after a burn-in of 5000 samples. The convergence is monitored based on the predictive likelihood of the test set at each MCMC iteration. The hyper parameters are the same as those in Section 5. The predictive log-likelihood of the test data are used to tune  $\alpha$  as described in Section 2.1.2. In our cross validation,  $\alpha = 0.01$  turns out to be optimal.

Figure 12 shows the estimated loadings using PFA, FBPFA and BMSFA. We cannot plot the loading matrices using the same color levels as the matrices are not comparable in value. However, all plots show two significant factors, with a moderately important third factor. The loading structure is similar across all the estimates, which provides additional support for one typical summary measure of the sum or weighted sum of all phthalates. For PFA, FBPFA, all the chemicals load on the first factor and the second factor is loaded on by the last four chemicals, namely MECPP, MEHHP, MEOHP, and MEHP. Figure 1 also suggests that these four chemicals are related to each other more than the others. This is not surprising, as MECPP, MEHHP, and MEOHP are oxidative metabolites of MEHP. We also compare PFA and FBPFA with BMSFA in terms of predictive log-likelihood in Table 7. As in the simulation study, PFA performs much better than BMSFA in terms of the predictive log-likelihood. In terms of predictive log-likelihood, FBPFA performs the best.

TABLE 7  
*Average predictive log-likelihood for different methods*

PFA for optimal $\alpha$	FBPFA	BMFA
4.12	5.02	-7.99

We calculate divergence scores and create the divergence matrix  $D$ . This is provided in Table 8 to infer about similarities across groups. To summarize  $D$ , we also plot Figure 13 which illustrates a network plot between different groups. The edge-width between two nodes  $(j, l)$  is calculated as  $60/d_{jl}$ . Thus, the edge-width is inversely proportional to the divergence statistic. Thicker edges imply greater similarity. Hence, this Figure implies that the N-H White group is the most different from the other four. This supports our one-way ANOVA results where we find that the phthalate concentra-

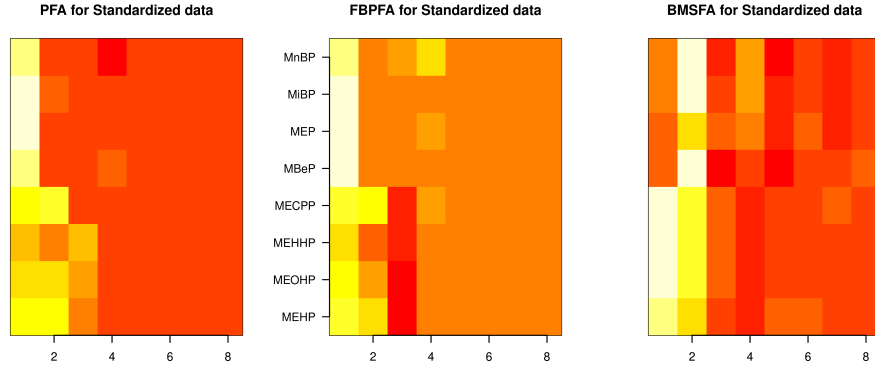


FIG 12. Comparison of estimated loading matrices with different methods. PFA estimates are based on  $\alpha = 1 \times 10^{-2}$ .

tion in group N-H White is significantly different from all the other groups. Also, Mex, OH and Other/Multi are the most similar ones. In Figure 2, the estimated loadings of the groups Mex, OH and Other/Multi are very similar. Estimated loading of N-H Black is also close to those. For the N-H White, there is one extra factor. Our results based on divergence scores also suggest similar distinctions among the groups. Also these results support our preliminary analysis, described in Section 2. In Table 9, we show square norm difference between the group specific loadings, estimated using BMSFA and the associated postprocessing. The  $(i, j)$ -th entry of the table is calculated as  $\sqrt{\sum_{lk} (A_{ill} - A_{jlk})^2}$ , where the matrices  $A_i$  and  $A_j$  are the estimated group-specific loadings for the groups  $i$  and  $j$  respectively using BMSFA. These numbers do not suggest similar clustering as we can conclude using our PFA method. All the groups seem to be almost equal distance apart from each other here.

TABLE 8  
Estimated divergence scores for different pairs of groups.

	Mex	OH	N-H White	N-H Black	Other/Multi
Mex	0.00	5.86	41.35	10.22	3.82
OH	5.86	0.00	40.93	8.38	4.45
N-H White	41.35	40.93	0.00	40.06	41.17
N-H Black	10.22	8.38	40.06	0.00	9.48
Other/Multi	3.82	4.45	41.17	9.48	0.00

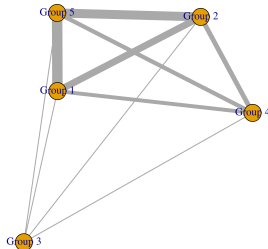


FIG 13. Network plot summarizing similarity between the groups based on the divergence metric where thicker edge implies smaller divergence score.

TABLE 9  
Square norm difference of the group-specific loadings, estimated using BMSFA.

	Mex	OH	N-H White	N-H Black	Other/Multi
Mex	0.00	0.75	0.70	0.59	0.78
OH	0.75	0.00	0.63	0.75	0.73
N-H White	0.70	0.63	0.00	0.68	0.84
N-H Black	0.59	0.75	0.68	0.00	0.91
Other/Multi	0.78	0.73	0.84	0.91	0.00

**7. Discussion.** Our over-arching goal was to develop a less brittle method for estimating factors that hold across similar datasets and groups within a dataset. In many applications, it is important to define a more generalizable set of factors, improving on the current status in which one often obtains dramatically different factors when fitting a factor model separately to different groups or using current additive ANOVA-type factor models. A primary innovation of the article is to incorporate a multiplicative perturbation of the data. As we have shown, this can be included in many different contexts - ranging from meta analysis, to multiple group data, to measurement error modeling, and even to obtain improved performance when there is no group or replicated structure in the data. We have demonstrated exciting improvements in performance in all of these settings.

It is our hope that the proposed method can be used directly by epidemiologists, and scientists in other fields, to obtain more generalizable factors in their applications. With this goal in mind, we have provided code for implementing the proposed approach at <https://github.com/royarkaprava/Perturbed-factor-model>. To make the method more broadly useful, there are a number of interesting extensions, some trivial and some less so. The

first is to adjust for covariates - this can be very easily done without modifying the fundamental approach with a simple tweak to the proposed Gibbs sampler. Another important modification is to allow data that are not simply all continuous variables but may be categorical or mixed categorical and continuous. This can rely on an underlying variable model, as is often used in factor analysis (see, for example, [Carvalho et al. \(2008\)](#); [Zhou et al. \(2015\)](#)). In this case, we would incorporate the perturbation in the underlying variables instead of in the observed data directly. Again, this leads to a minor modification of the proposed Gibbs sampling algorithm.

We conjecture that both the perturbation ideas and the idea of including heterogeneous factor variances to improve identifiability will have impact beyond the specific setting we have considered in this paper. For example, one natural extension is to non-linear factor models, such as Gaussian process latent variable models ([Lawrence, 2004](#); [Lawrence and Quiñonero-Candela, 2006](#)) and variational auto-encoders ([Kingma and Welling, 2013](#); [Pu et al., 2016](#)).

### Appendix.

#### *Proof of Theorem 5.*

PROOF. For  $q, q^* \in \mathcal{P}$  the space of probability measure, let the Kullback-Leibler divergences be given by

$$KL(q^*, q) = \int q^* \log \frac{q^*}{q}.$$

Let  $K(\kappa_0, \kappa)$  denote the Kullback-Leibler divergence

$$\sum_{j=1}^J KL(N(0, Q_j^{-1}[\Lambda \Sigma_2 \Lambda^T + \Sigma_1](Q_j^{-1})^T), N(0, Q_{j0}^{-1}[\Lambda_0 \Sigma_{20} \Lambda_0^T + \Sigma_{10}](Q_{j0}^{-1})^T)).$$

For our model, we have

$$K(\kappa_0, \kappa) = \frac{1}{2n} \left[ \sum_{j=1}^J -n_j \log |Q_{j0}^T \Sigma_0 Q_{j0} \{Q_j^T \Sigma Q_j\}^{-1}| \right. \\ \left. + n_j \text{tr}(Q_{j0}^T \Sigma_0 Q_{j0} \{Q_j^T \Sigma Q_j\}^{-1} - I_p) \right]$$

To prove Theorem 5, we rely on the following Lemma.



LEMMA 6. For any  $\epsilon > 0$ , there exists  $\epsilon_1 > 0, \epsilon_2 > 0$ , and  $\epsilon_{3j} > 0$  for  $j \in \{2, \dots, J\}$  such that  $\|\Lambda - \Lambda_0\|_F^2 \leq \epsilon_1^2$ ,  $\|\Sigma_2 - \Sigma_{20}\|_F^2 \leq \epsilon_2^2$  and  $\|Q_j - Q_{j0}\|_F^2 \leq \epsilon_{3j}^2$ , then we have

$$\begin{aligned} \Pi\{K(\kappa_0, \kappa) \leq \epsilon\} &\geq \\ \Pi\{\|\Lambda - \Lambda_0\|_F^2 \leq \epsilon_1^2, \|\Sigma_2 - \Sigma_{20}\|_F^2 \leq \epsilon_2^2, \|Q_j - Q_{j0}\|_F^2 \leq \epsilon_{3j}^2, j = 2, \dots, J\} \end{aligned}$$

Due to continuity of the functions such as determinant, trace and  $g(\cdot)$ , the above result is immediate following the proof of Theorem 2 in [Bhattacharya and Dunson \(2011\)](#). For our proposed priors, the prior probability of the R.H.S. of Lemma 6 is positive. Thus the prior probability of any Kullback-Leibler neighborhood around the truth is positive. This proves Theorem 5.  $\square$

*More exploratory analysis on NHANES data.* For each chemical level, we fit an one-way ANOVA model to analyse group-specific effects on each phthalate level separately.

TABLE 10  
For phthalate MnBP

	Estimate	Std. Error	t value	Pr(>  t )
(Intercept)	3.85	0.11	36.27	0.00
N-H Black	0.36	0.15	2.33	0.02
N-H White	-0.29	0.13	-2.26	0.02
OH	0.46	0.18	2.55	0.01
Other/Multi	-0.09	0.22	-0.41	0.68

TABLE 11  
For phthalate MiBP

	Estimate	Std. Error	t value	Pr(>  t )
(Intercept)	2.88	0.06	49.23	0.00
N-H Black	0.59	0.08	6.97	0.00
N-H White	-0.35	0.07	-4.98	0.00
OH	0.33	0.10	3.28	0.00
Other/Multi	-0.08	0.12	-0.68	0.50

**8. Acknowledgments.** This research was partially supported by grant R01-ES027498-01A1 from the National Institute of Environmental Health Sciences (NIEHS) of the National Institutes of Health (NIH).

**References.**

TABLE 12  
For phthalate MEP

	Estimate	Std. Error	t value	Pr(>  t )
(Intercept)	8.32	0.29	28.80	0.00
N-H Black	2.84	0.42	6.79	0.00
N-H White	-1.41	0.35	-4.02	0.00
OH	1.18	0.49	2.40	0.02
Other/Multi	-0.99	0.60	-1.64	0.10

TABLE 13  
For phthalate MBeP

	Estimate	Std. Error	t value	Pr(>  t )
(Intercept)	2.79	0.07	39.90	0.00
N-H Black	0.27	0.10	2.66	0.01
N-H White	-0.09	0.08	-1.05	0.29
OH	-0.01	0.12	-0.06	0.95
Other/Multi	-0.23	0.15	-1.57	0.12

- ASSMANN, C., BOYSEN-HOGREFE, J. and PAPE, M. (2016). Bayesian analysis of static and dynamic factor models: An ex-post approach towards the rotation problem. *Journal of Econometrics* **192** 190–206.
- BENJAMIN, S., MASAI, E., KAMIMURA, N., TAKAHASHI, K., ANDERSON, R. C. and FAISAL, P. A. (2017). Phthalates impact human health: epidemiological evidences and plausible mechanism of action. *Journal of hazardous materials* **340** 360–383.
- BHATTACHARYA, A. and DUNSON, D. B. (2011). Sparse Bayesian infinite factor models. *Biometrika* 291–306.
- CARVALHO, C. M., CHANG, J., LUCAS, J. E., NEVINS, J. R., WANG, Q. and WEST, M. (2008). High-dimensional sparse factor modeling: applications in gene expression genomics. *Journal of the American Statistical Association* **103** 1438–1456.
- DE VITO, R., BELLIO, R., TRIPPA, L. and PARMIGIANI, G. (2018). Bayesian Multi-study Factor Analysis for High-throughput Biological Data. *arXiv preprint arXiv:1806.09896*.
- FENG, Q., HANNIG, J. and MARRON, J. (2015). Non-iterative joint and individual variation explained. *arXiv preprint arXiv:1512.04060*.
- FENG, Q., JIANG, M., HANNIG, J. and MARRON, J. (2018). Angle-based joint and individual variation explained. *Journal of multivariate analysis* **166** 241–265.
- FRUEHWIRTH-SCHNATTER, S. and LOPES, H. F. (2018). Sparse Bayesian Factor Analysis when the Number of Factors is Unknown. *arXiv preprint arXiv:1804.04231*.
- JAMES-TODD, T. M., MEEKER, J. D., HUANG, T., HAUSER, R., SEELY, E. W., FERGUSON, K. K., RICH-EDWARDS, J. W. and MCELDRATH, T. F. (2017). Racial and ethnic variations in phthalate metabolite concentration changes across full-term pregnancies. *Journal of Exposure Science and Environmental Epidemiology* **27** 160.
- KIM, S. H. and PARK, M. J. (2014). Phthalate exposure and childhood obesity. *Annals of pediatric endocrinology & metabolism* **19** 69.
- KINGMA, D. P. and WELING, M. (2013). Auto-encoding variational bayes. *arXiv preprint arXiv:1312.6114*.
- LAWRENCE, N. D. (2004). Gaussian process latent variable models for visualisation of high dimensional data. In *Advances in neural information processing systems* 329–336.
- LAWRENCE, N. D. and QUIÑONERO-CANDELA, J. (2006). Local distance preservation in

TABLE 14  
For phthalate MECPP

	Estimate	Std. Error	t value	Pr(>  t )
(Intercept)	4.80	0.12	41.52	0.00
N-H Black	-0.44	0.17	-2.63	0.01
N-H White	-0.64	0.14	-4.56	0.00
OH	-0.25	0.20	-1.28	0.20
Other/Multi	-0.46	0.24	-1.89	0.06

TABLE 15  
For phthalate MEHHP

	Estimate	Std. Error	t value	Pr(>  t )
(Intercept)	3.83	0.10	36.85	0.00
N-H Black	-0.04	0.15	-0.26	0.79
N-H White	-0.39	0.13	-3.06	0.00
OH	-0.10	0.18	-0.56	0.58
Other/Multi	-0.26	0.22	-1.19	0.23

the GP-LVM through back constraints. In *Proceedings of the 23rd international conference on Machine learning* 513–520. ACM.

- LOCK, E. F., HOADLEY, K. A., MARRON, J. S. and NOBEL, A. B. (2013). Joint and individual variation explained (JIVE) for integrated analysis of multiple data types. *The Annals of Applied Statistics* **7** 523.
- LOPES, H. F. and WEST, M. (2004). Bayesian model assessment in factor analysis. *Statistica Sinica* 41–67.
- PISON, G., ROUSSEEUW, P. J., FILZMOSER, P. and CROUX, C. (2003). Robust factor analysis. *Journal of Multivariate Analysis* **84** 145–172.
- PU, Y., GAN, Z., HENAO, R., YUAN, X., LI, C., STEVENS, A. and CARIN, L. (2016). Variational autoencoder for deep learning of images, labels and captions. In *Advances in neural information processing systems* 2352–2360.
- ROČKOVÁ, V. and GEORGE, E. I. (2016). Fast Bayesian factor analysis via automatic rotations to sparsity. *Journal of the American Statistical Association* **111** 1608–1622.
- ROY, A., SCHAICH-BORG, J. and DUNSON, D. B. (2019). Bayesian time-aligned factor analysis of paired multivariate time series. *arXiv preprint arXiv:1904.12103*.
- SARKAR, A., PATI, D., CHAKRABORTY, A., MALLICK, B. K. and CARROLL, R. J. (2018). Bayesian semiparametric multivariate density deconvolution. *Journal of the American Statistical Association* **113** 401–416.
- SCHWARTZ, L. (1965). On bayes procedures. *Zeitschrift für Wahrscheinlichkeitstheorie und verwandte Gebiete* **4** 10–26.
- SEBER, G. A. (2009). *Multivariate observations* **252**. John Wiley & Sons.
- TAYLOR, K. W., TROESTER, M. A., HERRING, A. H., ENGEL, L. S., NICHOLS, H. B., SANDLER, D. P. and BAIRD, D. D. (2018). Associations between personal care product use patterns and breast cancer risk among white and black women in the sister study. *Environmental health perspectives* **126** 027011.
- WEISSENBURGER-MOSER, L., MEZA, J., YU, F., SHIYANBOLA, O., ROMBERGER, D. J. and LEVAN, T. D. (2017). A principal factor analysis to characterize agricultural exposures among Nebraska veterans. *Journal of Exposure Science and Environmental Epidemiology* **27** 214.

TABLE 16  
For phthalate MEOHP

	Estimate	Std. Error	t value	Pr(>  t )
(Intercept)	3.11	0.08	39.04	0.00
N-H Black	-0.06	0.12	-0.54	0.59
N-H White	-0.33	0.10	-3.39	0.00
OH	-0.11	0.14	-0.83	0.41
Other/Multi	-0.26	0.17	-1.54	0.12

TABLE 17  
For phthalate MEHP

	Estimate	Std. Error	t value	Pr(>  t )
(Intercept)	1.58	0.04	35.44	0.00
N-H Black	0.03	0.06	0.44	0.66
N-H White	-0.25	0.05	-4.57	0.00
OH	0.01	0.08	0.10	0.92
Other/Multi	0.00	0.09	0.02	0.99

ZHANG, Y., MENG, X., CHEN, L., LI, D., ZHAO, L., ZHAO, Y., LI, L. and SHI, H. (2014). Age and sex-specific relationships between phthalate exposures and obesity in Chinese children at puberty. *PloS one* **9** e104852.

ZHOU, J., BHATTACHARYA, A., HERRING, A. H. and DUNSON, D. B. (2015). Bayesian factorizations of big sparse tensors. *Journal of the American Statistical Association* **110** 1562–1576.

ARKAPRAVA ROY  
ISAAC LAVINE  
DEPARTMENT OF STATISTICS  
DUKE UNIVERSITY  
DURHAM, NC  
E-MAIL: [arkaprava.roy@duke.edu](mailto:arkaprava.roy@duke.edu)  
[isaac.lavine@duke.edu](mailto:isaac.lavine@duke.edu)

AMY HERRING  
DAVID B. DUNSON  
DEPARTMENT OF STATISTICS  
DUKE UNIVERSITY  
DURHAM, NC  
E-MAIL: [amy.herring@duke.edu](mailto:amy.herring@duke.edu)  
[dunson@duke.edu](mailto:dunson@duke.edu)